ChemComm

Chemical Communications

ROYAL SOCIETY
OF CHEMISTRY

FEATURE ARTICLE
Xiaosheng Yan, Yun-Bao Jiang *et al.*
Supramolecular helices from helical building blocks *via*
head-to-tail intermolecular interactions

Supramolecular helices from helical building blocks *via* head-to-tail intermolecular interactions

Xiaosheng Yan, [ID] * Peimin Weng, Di Shi and Yun-Bao Jiang [ID] *

Supramolecular helices from helical building blocks represent an emerging analogue of the α-helix. In cases where the helicity of the helical building block is well propagated, the head-to-tail intermolecular interactions that lead to the helix could be enhanced to promote the formation and the stability of the supramolecular helix, wherein homochiral elongation dominates and functional helical channel structures could also be generated. This feature article outlines the supramolecular helices built from helical building blocks, *i.e.*, helical aromatic foldamers and helical short peptides that are held together by intermolecular π–π stacking, hydrogen/halogen/chalcogen bonding, metal coordination, dynamic covalent bonding and solvophobic interactions, with emphasis on the influence of efficient propagation of helicity during assembly, favouring homochirality and channel functions.

Introduction

Building supramolecular helical assemblies to mimic biological helices,[1] *i.e.*, the DNA double helix[2] and protein α-helix,[3] will help in understanding the structural and interaction factors that govern the formation of those helices and thereby help in the development of new artificial supramolecular helices of diverse structures and functions. In terms of the helicity, the helical columnar stacking of base-pairs affords the global helicity of the

Department of Chemistry, College of Chemistry and Chemical Engineering, The MOE Key Laboratory of Spectrochemical Analysis and Instrumentation, and iChEM, Xiamen University, Xiamen 361005, China. E-mail: xshyan@xmu.edu.cn, ybjiang@xmu.edu.cn

DNA double helix, which inspires the creation of supramolecular helical assemblies through helical columnar stacking of planar π-conjugated building blocks, for example, trialkylbenzene-1,3,5-tricarboxamide discotics,[4] porphyrins,[5] perylene bisimides[6] and merocyanine dyes.[7] For the α-helix in proteins, however, its helicity originates from the helical peptide backbone of the α-turn structure. The α-helix can therefore be alternatively viewed as a helix from helical fragments, the α-turns that are linked by amide bonds in the head-to-tail pattern.[3] The hydrogen bonds between neighbouring α-turns provide additional interactions to further stabilize the α-helix structure. This offers a new inspiration for the creation of stable supramolecular helices by using helical building blocks to be held together into supramolecular helices *via* head-to-tail intermolecular interactions (Fig. 1).

Xiaosheng Yan obtained his Bachelor's degree in applied chemistry from Huazhong Agricultural University in 2010, and his PhD degree in analytical chemistry from Xiamen University in 2016 under the supervision of Professor Yun-Bao Jiang. Now he is a postdoctoral research associate in Prof. Yun-Bao Jiang's group. His research interests are centered on the folding and assembly of short peptides, the supramolecular chirality of aggregates, halogen/chalcogen-bonding-driven supramolecular helices, and spontaneous chiral resolution.

Xiaosheng Yan

Peimin Weng received her Bachelor's degree in chemistry from Fuzhou University in 2018. She joined Prof. Yun-Bao Jiang's group in Xiamen University in September 2018 as a PhD student. Her current research focuses on the development of functional supramolecular helices from folded short peptides.
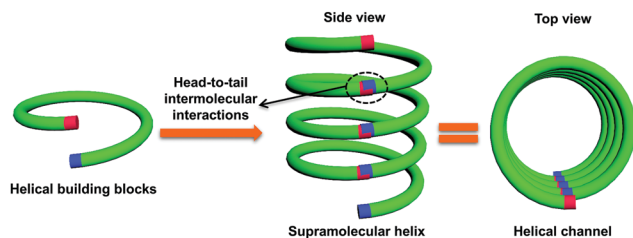
Peimin Weng

Fig. 1 Schematic illustration of the supramolecular helix from helical building blocks through head-to-tail intermolecular interactions, which may lead to a helical channel.

From that perspective it is of interest to examine how the helical conformation of the building block affects the supramolecular helical assembly. First, the helical building block possesses intrinsic helicity, and propagation of this helicity would enhance the matched intermolecular interactions and likely promote the formation of stable supramolecular helices. This assembling mechanism may open an avenue towards single-strand supramolecular helices following, in the majority of cases, a single-point interaction. Second, homochiral elongation is preferred in the formation of such supramolecular helices, as what is happening in the DNA duplex from all D-sugar moieties or in the α-helix of all L-amino acid residues allows good propagation of the helicity of the helical building block. This homochirality may result in a chiral amplification effect, such as spontaneous chiral resolution[8] and interesting characteristics in supramolecular chirality in terms of the "majority-rules effect" and "sergeants-and-soldiers" principle.[9,10] Third, this assembly process may generate helical channels (Fig. 1), which are useful for molecular encapsulation, recognition and transportation.

Supramolecular helices are thus expected to be created from helical building blocks *via* head-to-tail intermolecular interactions, establishing a platform for the creation of α-helix mimics. This essential concept, however, has not received much attention, despite the fact that helical building blocks such as helical aromatic foldamers and helical short peptides have indeed been employed to build supramolecular helices through intermolecular interactions such as π–π stacking, hydrogen bonding, and metal coordination. We therefore consider that a summary of these supramolecular helices from helical building blocks may provide a general overview of the state of the art and inspire researchers so that many such supramolecular helices of highly diverse structures and functions could be made and their applications explored. In this feature article, we first describe the concept of the "propagation of helicity", which is followed a review of supramolecular helices built from helical aromatic foldamers and helical short peptides in which helicity propagation has played a role. Finally, we discuss the different viewpoints on this subject. The supramolecular helices summarized here are limited to helical polymeric chains from infinite helical building blocks that are linked by head-to-tail interactions, as those shown in Fig. 1, and helicates in linear or circular forms from finite helical building blocks are not included.[1,11]

Propagation of helicity

A factor in the formation of supramolecular helices from helical building blocks is the role of the "propagation of helicity". In cases where the helicity of the building block is well propagated upon intermolecular interactions between the building blocks that lead to the helices, the ease of formation and the stability of the formed supramolecular helices could be increased.

A vivid example of the "propagation of helicity" in daily life is ribbon gymnastics in the Olympic Games. The ribbon used is composed of a rigid stick and a flexible ribbon. The helicity is created by the gymnast by rotating the stick and it is meanwhile transferred from the stick to the ribbon, which is subsequently propagated along the ribbon to result in a beautiful helical ribbon, wherein homochirality dominates (Fig. 2a).

Di Shi is a PhD student in Prof. Yun-Bao Jiang's group in Xiamen University, China. She received her Bachelor's degree in materials chemistry in 2018 from Huaqiao University. Her research interests include the development of chalcogen bonding-driven supramolecular helices and the synthesis and applications of macrocyclic molecules from folded short peptides.

Di Shi

Yun-Bao Jiang is a Professor of Chemistry in the College of Chemistry and Chemical Engineering, Xiamen University, China. He received his PhD from Xiamen University in 1990 under the supervision of Professor Guo-Zhen Chen. He was awarded the distinguished young investigator grant by the NSF of China and has led innovation research teams that are financially supported by the Ministry of Education and the NSF of China. His current research interests include the design and applications of chemical sensors and hierarchical self-assembling systems, with a focus on supramolecular photophysics, metallophilic interactions and supramolecular chirality.
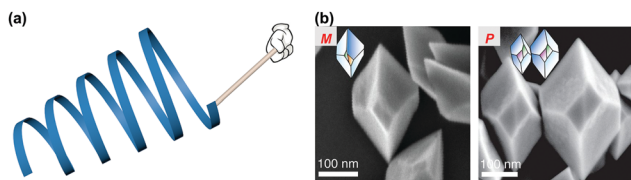
Yun-Bao Jiang

Fig. 2 (a) Schematic illustration of helical ribbon in ribbon gymnastics, showing the propagation of helicity along the ribbon. (b) Left-handed (*M*) and right-handed (*P*) bipyramids of chiral tellurium nanocrystals, stemming from screw dislocation in the crystal nuclei, in that the helicity is propagated to yield chirally shaped crystals. Adapted with permission from ref. 14. Copyright 2021 American Association for the Advancement of Science.

The "propagation of helicity" is also illustrated in the formation of crystals of chiral shapes. In addition to intrinsic chiral crystal structures and by the induction of chiral additives, chiral crystal shapes can also stem from screw dislocations in crystal nuclei, which lead to a more reactive front for crystal growth.[12,13] This means that the propagation of the helicity of crystal nuclei facilitates the growth of crystals leading to chirally shaped crystals. This has recently been demonstrated by Alivisatos *et al.*[14] in their investigations into the chiral polyhedral shapes of tellurium nanocrystals obtained under low supersaturation conditions (Fig. 2b).[14,15]

Promotion of the supramolecular helix from helical building blocks by the "propagation of helicity" can be viewed as a cooperative effect of intra- and inter-molecular interactions.[16] The former maintain the helical conformation of the building blocks and pre-organize at optimal positions the sites in the building blocks for their intermolecular interactions that lead to the supramolecular helix, wherein the helical conformation of the building blocks is further stabilized.

Homochiral elongation along the axis of the helix is favoured since that allows the good "propagation of helicity", which may lead to the experimental observation of spontaneous resolution,[8] the "majority-rules effect" and the "sergeants-and-soldiers" principle,[9,10] which will be discussed in later examples. Those observations imply the occurrence of chiral amplification, an intriguing phenomenon that not only relates to the origin of natural homochirality but also it is useful for the preparation of practically important enantiopure products. Therefore, the "propagation of helicity" could be an effective mechanism towards chiral amplification, while the observation of chiral amplification during the formation of supramolecular helices from helical building blocks could be an indication of the "propagation of helicity".

Helical aromatic foldamers as building blocks

Synthetic foldamers were initially developed to mimic the sophisticated structures and functions of natural proteins and RNA molecules that adopt specific compact conformations.[17] Aromatic foldamers, an important type of synthetic abiotic foldamer, tend to fold into specific helical conformations maintained by their rigid aromatic backbone, intramolecular

hydrogen bonding and aromatic π–π stacking.[18–21] When structural matching is reached so that good propagation of the helicity of the helical aromatic backbone is allowed, the foldamers tend to form elongated supramolecular helices, most of which have cavities that function as channels for molecular recognition and transportation (Fig. 1).

An insightful piece of work on this subject is the investigation by Moore *et al.* on the helical polymerization of *m*-phenylene ethynylene (*m*PE) oligomers. While adopting a random conformation in CHCl₃, *m*PE oligomers **1** of sufficient length ($n > 8$) are able to fold in an ordered helical conformation in the polar solvent CH₃CN, showing increased stability as a result of solvophobic interactions and intramolecular π–π stacking (Fig. 3a).[22] The stability gained from folding is capable of promoting the formation of supramolecular helical polymers from the bis-functionalized *m*PE oligomers, in cases where the building block backbone chain is long enough (a tetramer or longer) to allow for a folding-driven helical sense, or helicity upon dimerization.[23–27] For example, the bisimine-functionalized *m*PE tetramers **2** and **3** undergo imine metathesis polymerization in the presence of oxalic acid (Fig. 3b).[24] In the less polar solvent CHCl₃, the major components in the equilibrium state are the starting materials, dimers, trimers and a tiny amount of oligomers, whereas in polar CH₃CN, long polymers of high molecular weight are produced. This is ascribed to the folding of *m*PE oligomers in the polar solvent CH₃CN, which allows efficient intermolecular aromatic π–π stacking to stabilize the formed helical polymers, thereby
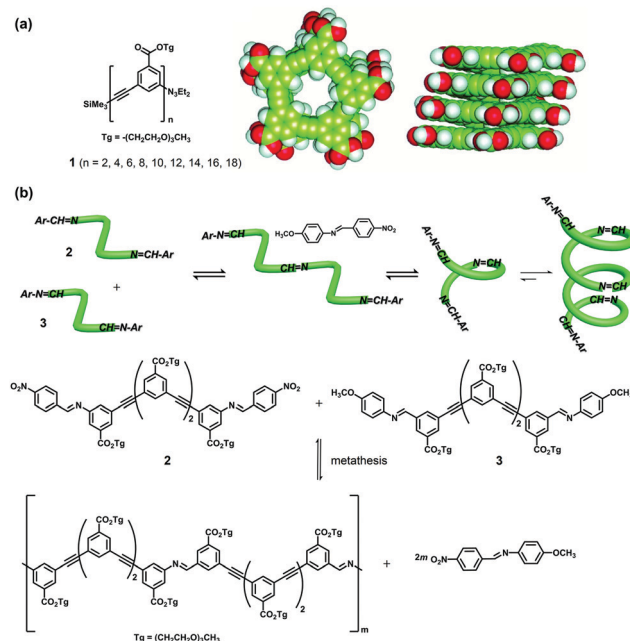

Fig. 3 (a) Molecular structure of *m*-phenylene ethynylene (*m*PE) oligomers **1** and molecular modelling of the helical conformation of the octadecamer ($n = 18$) in which T_g = H and the end groups are removed. Adapted with permission from ref. 22. Copyright 1997 American Association for the Advancement of Science. (b) Imine metathesis polymerization between bisimine-functionalized *m*PE oligomers **2** and **3**. Adapted with permission from ref. 24. Copyright 2002 American Chemical Society.
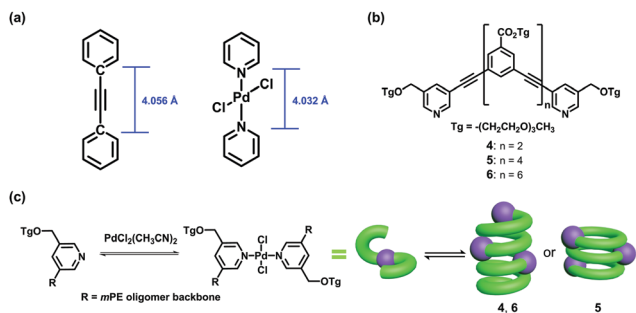
Fig. 4 (a) Structural illustration of the average C–C distance in diphenyl-lacetylene and the N–N distance in the pyridine–palladium–pyridine complex. (b) Molecular structure of mPE oligomers **4–6**. (c) Pd^{2+}–Pyridine coordination leads to supramolecular helices from **4** and **6**, but the π-stacked columnar polymer from **5**. Adapted with permission from ref. 27. Copyright 2006 American Chemical Society.

promoting the formation of longer helical polymeric chains (Fig. 3b). This can be well supported by the nucleation–elongation mechanism that governs the polymerization process in CH$_3$CN, explaining the cooperative imine metathesis and folding-driven aromatic π–π stacking in helical polymers.[25] This cooperativity shares a similarity with the concept of "propagation of helicity" that we suggested, so that the folding-driven helicity of the helical dimers could be further propagated through imine metathesis to form longer helical polymers (Fig. 3b).

Alternatively, the pyridine group was introduced at one or both ends of the mPE oligomers, generating supramolecular helical dimers[26] or polymers[27] upon coordination with Pd^{2+}. The N–N distance (4.032 Å) in the pyridine–Pd^{2+}–pyridine complex is close to the average bond length of C–C in the diphenylacetylene structure, 4.056 Å (Fig. 4a).[26] Therefore, pyridine–Pd^{2+} coordination matches the mPE backbone well, enabling the formation and stabilization of supramolecular helices from the mPE oligomers. This is insightful for designing the intermolecular interactions that link the helical building blocks into supramolecular helices. In the presence of Pd^{2+}, the mPE tetramer **4** and octamer **6** form supramolecular helical polymers in CH$_3$CN under the nucleation–elongation mechanism of the cooperative pyridine–Pd^{2+} coordination and intra-/inter-molecular π–π stacking, whereas hexamer **5** forms macrocycles, followed by columnar stacking (Fig. 4b and c).[27] This shows the dramatic influence of the backbone chain length of the foldamers on the formed supramolecular structure.
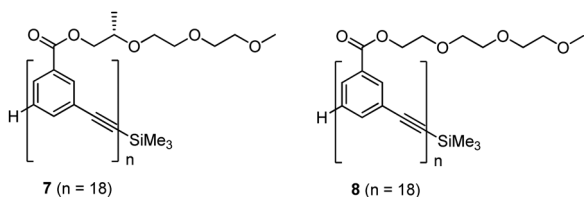
In the absence of dynamic covalent bonding and metal coordination, longer helical mPE oligomers such as octadecamers **7** and **8** can also assemble into supramolecular helical polymers in CH$_3$CN/H$_2$O solutions, driven by solvophobic and intra-/intermolecular π–π interactions.[28] Interestingly, the CD intensities

of the mixed oligomers of chiral **7** and achiral **8** in 60 : 40 (v/v) CH$_3$CN/H$_2$O solution depend non-linearly on the molar ratio of the chiral component **7**, exhibiting a "sergeants-and-soldiers" principle that the chirality is transferred from chiral **7** to achiral **8** during their copolymerization. It is proposed that propagation of the helicity of the chiral mPE oligomer favours homochiral elongation, driving the achiral mPE components to adopt the same helical sense defined by the chiral components and thereby the occurrence of chiral amplification. This agrees well with the homochiral properties observed with supramolecular helices built from pure helical building blocks, which will be discussed later.
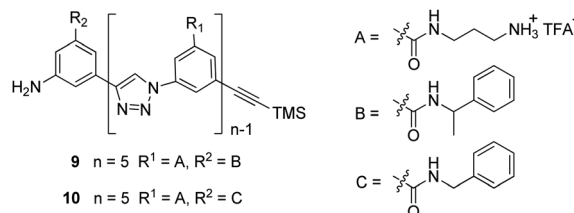
The folding and aggregation mechanism and the "sergeants-and-soldiers" principle has also been illustrated in the cationic oligo(phenylene-1,2,3-triazole) compounds **9** and **10** reported by the Jiang group.[29] While prevailing as a random-coiled conformation in CH$_3$OH in their monomer form, oligomers **9** and **10** take a helical conformation in aqueous solution, driven by solvophobic and van der Waals interactions, which leads to their further stacking into supramolecular helices in a head-to-tail pattern, followed by intertwining into high-order super-structures. Interestingly, in pure water the CD intensities of mixtures of chiral **9** and achiral **10** depend linearly on the molar ratio of chiral **9**, whereas the dependence becomes non-linear in 25 : 75 (v/v) CH$_3$OH/H$_2$O solution, indicative of the "sergeants-and-soldiers" principle. This is ascribed to their compact aggregation in pure water, whereas it is looser in the CH$_3$OH/H$_2$O mixture. The observation of chiral amplification implies that the propagation of helicity is operative, which promotes the formation of supramolecular helices in aqueous solutions. The helical cavity from oligomer **9** can bind halide anions, such as Cl$^-$ and F$^-$, in aqueous solution, which prevents its aggregation, presumably due to electrostatic repulsion between the halide anions.

While the backbone of the mPE oligomer or oligo(phenylene-1,2,3-triazole) is flexible, its folding cooperatively promotes the formation of supramolecular helices; foldamers of rigid aromatic backbones with fixed helical conformation are alternative helical building blocks for supramolecular helices. In 2000, Lehn and co-workers[30] developed a heterocyclic oligomer **11** consisting of alternating pyridine–pyridazine units. The pyridine–pyridazine structural motif prefers to adopt the trans-conformation, driving oligomer **11** into the lock-washer-shaped helical structure in which one turn consists of twelve heterocycles with an outside diameter of about 25 Å and an inner cavity of about 8 Å (Fig. 5a) in which intramolecular π–π stacking between two terminal pyridine rings provides additional stabilization. Helical compound **11** self-aggregates in CHCl$_3$ to form a supramolecular helix through twelve pairs of π–π interactions between two neighboring
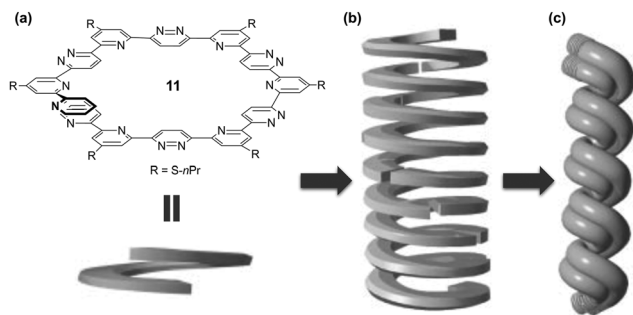
Fig. 5 Hierarchical assembly of helical pyridine–pyridazine oligomer **11** into supramolecular helix and coiled-coil chiral fibers. Adapted with permission from ref. 30. Copyright 2000 Wiley-VCH.

molecules (Fig. 5b), together with π–π stacking between helices, to form coiled-coil chiral fibers in CH_2Cl_2 and pyridine (Fig. 5c).[30] Surprisingly, upon sonication and aging, chiral fibers with a helical pitch of *ca.* 10 nm from **11** in CH_2Cl_2 are optically active and show a majority of one helical sense, exhibiting a symmetry breaking and spontaneous resolution indicative of the chiral amplification.[31] This was attributed to a secondary nucleation growth mechanism in which the helical conformation of **11** facilitates its homochiral growth that allows optimal aromatic π–π stacking between two helical oligomer-**11** molecules of the same handedness, allowing the propagation of helicity. Upon addition of diethyl D- or L-tartrate, an induced CD signal is observed, meaning that one handedness of the chiral fibers is selectively generated.
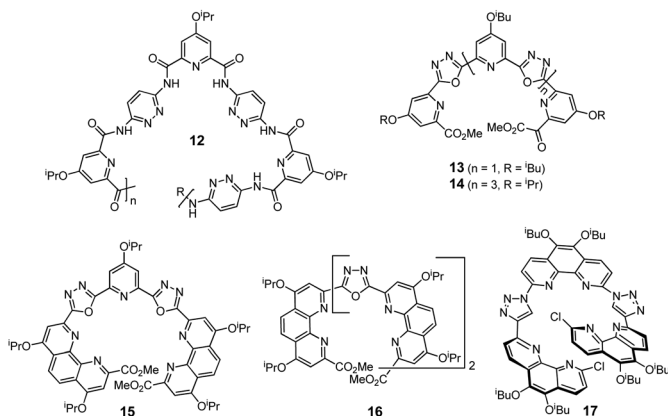
It is particularly interesting that the hollow tube structure of the supramolecular helices from the lock-washer-shaped foldamer **11** (Fig. 5b) opens up a way for developing artificial channels for molecular recognition and transportation. For example, Dong and co-workers[32] created a supramolecular helix of the channel structure from helical pyridine–pyridazine oligomer **12**, *via* intermolecular π–π interactions. Because of the nitrogen-rich nature of the cavity of diameter *ca.* 6 Å, the channel recognizes and transports alkali ions Li^+, Na^+, K^+ and Rb^+ with a similar sensitivity and activity. Significantly, the addition of CF_3COOH and subsequent neutralization by Et_3N result in a reversible transformation between the folded and unfolded conformations of oligomer **12**, thereby allowing a reversible collection and triggered-release of alkali ions using the supramolecular channel.

Selectivity is an important advantage of natural channels. In 2017, Dong and co-workers[33] reported highly selective artificial K^+ ion channels from the helical pentamer **13** and nonamer **14** that contain the 2,5-bis(2-pyridyl)-1,3,4-oxadiazole motif. These form, *via* intermolecular π–π stacking, supramolecular helices of similar channel sizes, of diameter *ca.* 3.8 Å,[34] and similar cavity environments. The resultant hollow helices of **13** and **14** contain contiguous binding sites for K^+ ions, forming electron-rich pseudo-macrocycles of K^+ ion affinity and therefore enabling membrane-penetrating K^+ transportation. In the CH_3CN/H_2O mixtures, the binding constant of **14** with K^+ (2351, 2 : 3 binding ratio) is higher than that of **13** (614, 1 : 1 binding ratio). These are of the same order of their K^+-transport activities (EC_{50} of 4.1 μM for **14**, 10.5 μM for **13**). It is notable that these artificial channels exhibit high K^+/Na^+ selectivity ratios during transmembrane ion transportation, *e.g.*, the K^+/Na^+ selectivity of pentamer **13** is 9.1, while that of nonamer **14** is 22.5. It is proposed that the helical elongation increases the ion coordination number of the channel, enhancing the K^+ binding and consequently the K^+/Na^+ selectivity ratio.[33]

Tuning the channel size could be another way to mediate the selectivity and activity of ion transportation. Through a sequence-substitution strategy using pyridine, phenanthroline and oxadiazole moieties, Dong and co-workers[34] recently designed helical foldamers **15** and **16**. The hollow helix from **15** exhibits a channel size of *ca.* 2.7 Å, smaller than that of **14** (3.8 Å), which is therefore more matched to the size of K^+ (2.76 Å) and shows a much higher K^+-transport activity (EC_{50} = 35 nM) and a higher K^+/Na^+ selectivity of 32.6. While the channel size of the hollow helix from foldamer **16** is decreased to 2.3 Å, the selectivity is shown for the smaller Na^+ (2.04 Å), representing a rare Na^+-preferential channel, where the Na^+/K^+ selectivity is 5.2 and EC_{50} for the Na^+-transport activity is 280 nM. The importance of the channel size in ion-transport activity and selectivity is nicely proven. Supramolecular hollow helices from helical aromatic foldamers could actually be promising artificial channels in therapeutic applications, because of these good activity and selectivity properties.

Inspired by the controllable natural gated ion channels, Zhu and co-workers[35] developed a reversible ligand-gated ion channel using the helical aromatic foldamer **17**, which consists of alternating units of 1,10-phenanthroline and 1*H*-1,2,3-triazole. *Via* intermolecular π–π interactions, helical **17** molecules stack into a hollow single helix with a short pitch of 3.5 Å and a cavity of 3.6 Å, which, embedded in the lipid bilayers, acts as a channel to transport protons and alkali ions. The addition of Cu^+ results in disassembly of the hollow single helix and the formation of a new, intertwined double helix without an inner cavity, losing the function of a channel. With subsequent addition of $NH_3 \cdot H_2O$, which coordinates Cu^+ ions, the hollow single helix with channel activity is recovered (Fig. 6). The helical aromatic foldamer therefore undergoes a dynamic transition between single and double helical assembly, establishing a reversible ligand-gated ion channel for use in the development of intelligent artificial nanochannels.

Hollow helices from aromatic foldamers, when made in large size, can transport other species, for example, the biological
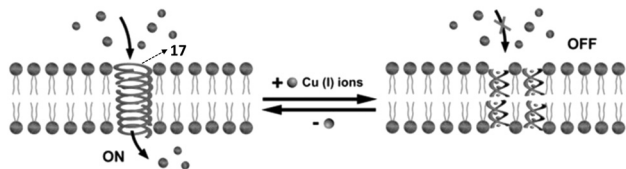
Feature Article

Fig. 6 Reversible ligand-gated ion channel of **17** triggered by Cu$^+$ and NH$_3$·H$_2$O. Adapted with permission from ref. 35. Copyright 2020 Wiley-VCH.
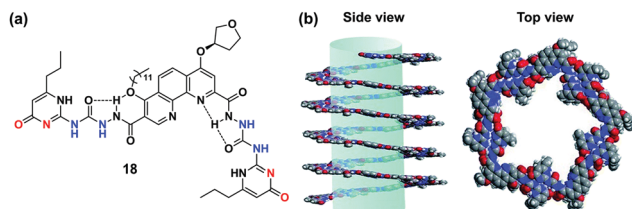

Fig. 7 (a) Molecular structure of aromatic hydrazide foldamer **18**. Blue atoms are hydrogen-bonding donors, while red ones are acceptors. (b) Molecular modeling of hollow helices from **18**. Adapted with permission from ref. 36. Copyright 2019 Royal Society of Chemistry.

fuel molecule glucose. Dong and co-workers[36] designed an aromatic hydrazide foldamer **18** in which two ureidopyrimidinone moieties are linked by a phenanthroline moiety (Fig. 7a). Following intermolecular quadruple AADD·DDAA hydrogen-bonding and π–π stacking, the shape-persistent foldamer **18** self-assembles into hollow helices (Fig. 7b), forming a large cavity of diameter *ca.* 2.6 nm that allows glucose transportation across the lipid bilayers with an excellent efficiency. In the presence of 4.0 mol% **18** (building block to lipid molar ratio), glucose entrapped in the large unilamellar vesicles is completely released in 30 min. Therefore, controlling the cavity size of the hollow helix from the helical aromatic foldamer can be used to transport target species of varying sizes.

Interestingly, these unique properties of supramolecular helices consisting of helical aromatic foldamers, such as homochiral growth, spontaneous resolution and the helical channel structure, have also been illustrated in helices built from pyridine-based aromatic amide foldamers by Zeng's group.[37–39] Because of the strong intramolecular hydrogen bonding between the pyridine N-atom and the amide –NH proton, achiral rigid pentamer **19** (Fig. 8a) adopts a helical conformation with a full helical turn.[37] Through intermolecular V-shaped hydrogen bonding between its two sticky ends (the C-terminal ester O-atom and the N-terminal Cbz aromatic proton, 1.1 kcal mol^{-1}, Fig. 8b), as well as the energetically more favoured fully overlapping π–π stacking (30 kcal mol^{-1}), the achiral foldamers efficiently stack on top of each other, forming a single-handed supramolecular helix (Fig. 8c), which, following edge-to-edge contacts between neighboring helices, assembles into ordered chiral 3D crystal lattices. Therefore, the achiral aromatic foldamer **19** undergoes spontaneous resolution to form enantiopure single-handed helical structures through crystallization, despite the absence of a chiral auxiliary or an external stimulus. Favoured homochiral growth that results from good propagation of the helicity of the helical aromatic backbone was taken to explain this chiral amplification effect.
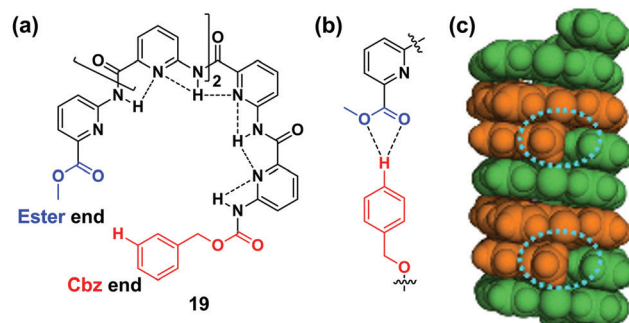

Fig. 8 (a) Molecular structure of pyridine-based helical foldamer **19**. (b) Intermolecular V-shaped hydrogen bonding. (c) Crystal structure of single-handed supramolecular *M*-helix from **19** through intermolecular hydrogen bonding and full-overlap π–π stacking. Adapted with permission from ref. 37. Copyright 2012 Royal Society of Chemistry.

Subsequently, Zeng and co-workers[38] designed the aromatic foldamer **20** (Fig. 9a), using a rigid phenyl group to replace the more flexible Cbz group in **19**. The formed hollow helices from **20** exhibit a pore diameter of 2.8 Å that matches well with the diameter of the water molecule (Fig. 9b), allowing for the rapid and selective transport of water molecules by the well-defined hydrogen-bonding donors (amide hydrogen atoms) and acceptors (pyridine groups) that are good for water binding. The crystal structure shows that the 1D hollow helices are exclusively made up of helical foldamers of the same handedness in which the intermolecular weak, while indispensable, hydrogen bonding between the two sticky ends (2.26 kcal mol^{-1}) and strong aromatic π–π stacking (29.75 kcal mol^{-1}) function cooperatively, and are
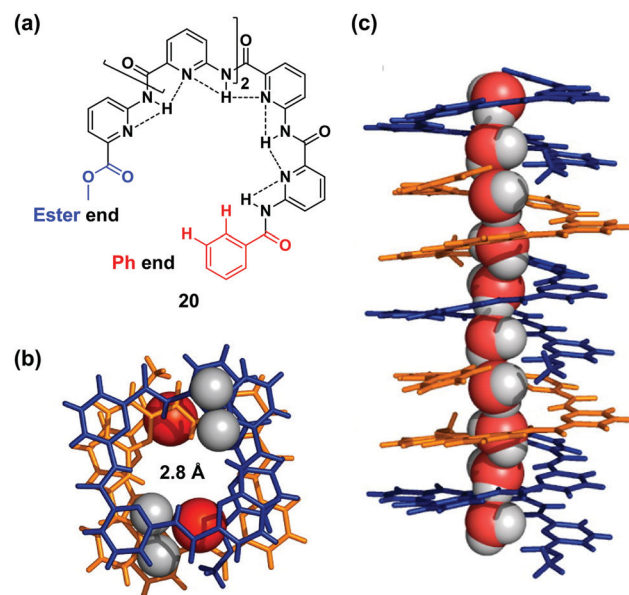

Fig. 9 (a) Molecular structure of pyridine-based helical aromatic amide foldamer **20**. (b) Intermolecular hydrogen bonding and fully overlapping π–π stacking in the crystals, showing a pore diameter of 2.8 Å. (c) Crystal structure of single-handed supramolecular *P*-helix from **20** in which a water chain is formed. Adapted with permission from ref. 38. Copyright 2014 American Chemical Society.

geometrically compatible with the helical backbone of **20**, allowing the good propagation of helicity of the helical backbone. Within the 1D helices, 1D water chains are accommodated with the same helix handedness, four water molecules per turn with a pitch of 10.32 Å (Fig. 9c). Each water molecule interacts with the hollow helix of **20** via five hydrogen bonds, including two amide –NH protons, two pyridine N atoms and one ester O atom. Each water molecule in the water chain is also stabilized by two adjacent water molecules via two intermolecular hydrogen bonds. The hollow helices from **20** can function as channels to transport protons and H_2O molecules in the case of a proton gradient existing across the lipid membranes, while there is no activity toward other ionic species. These supramolecular helices from helical aromatic foldamers are therefore shown to be capable of mimicking aquaporins for hosting water chains in the nano-channels and enabling water transportation.

As an interesting analogue of hydrogen bonding, halogen bonding has also been extensively employed to build supramolecular assemblies.[40,41] Li and co-workers[42] synthesized aromatic amide foldamers **21–24**, which all adopt a crescent shape because of the intramolecular hydrogen bonding. One end of the molecules **21–23** is equipped with a pyridine group, while the other is attached with either a CF_2I or a fluorinated iodobenzene group, allowing intermolecular head-to-tail C–I···N halogen bonding that is able to link foldamer molecules into supramolecular single-strand *P*- and *M*-helices, with a pitch of 17.5 Å, 22.4 Å and 17.1 Å, respectively. Aromatic π–π stacking occurs between the formed single helices, driving the formation of supramolecular double (**21**, **22**) and quadruple (**23**) helices in the crystalline state. This is different from the aforementioned supramolecular helices from foldamers **2–20** in which aromatic π–π stacking occurs mainly within the same helix to stabilize it. Foldamer **24**, which bears a pyridine group at each end, co-assembles with ICF_2CF_2I (**25**), giving rise to a single-stranded *P*- or *M*-helix through C–I···N halogen bonding with a pitch of 20.1 Å, and further into double-stranded helices and quadruple helical arrays by the additional π–π stacking between the helices. With diiodo-compound **26** (1,4-diiodotetrafluorobenzene), however, it binds to foldamer **24** to form 2+2 macrocycles via four C–I···N halogen bonds, which further stack to a supramolecular tube in which two neighbouring macrocycles encapsulate one molecule of **26** through two C=O···I halogen bonds.[43] Halogen bonding is shown to be a useful driving force to lead to supramolecular helices and macrocycles from aromatic foldamers.
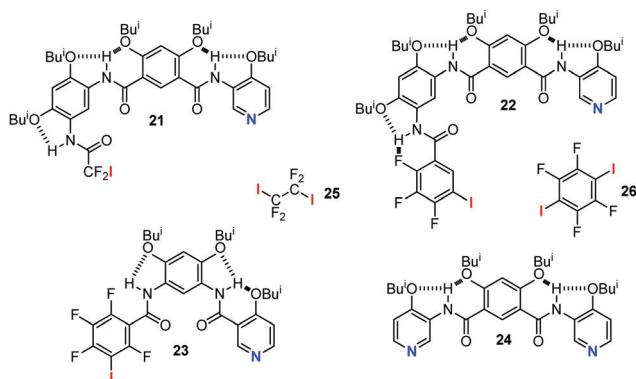
It now appears that aromatic foldamers are potential helical building blocks for the formation of supramolecular helices, through intermolecular aromatic π–π stacking, hydrogen- and/or halogen-bonding, metal–cation coordination and dynamic covalent bonding, which may function in a cooperative manner to bring about good propagation of the helicity of the helical backbone occurs. The formation of the supramolecular helix is therefore facilitated so that homochiral elongation is observed. Structurally, these supramolecular helices from helical aromatic foldamers prefer to adopt a pore or channel structure, to encapsulate, recognize and transport a variety of ions and neutral species such as glucose and water, while their selectivity and activity can be regulated by changing the constitutional structure of the backbone.

Helical short peptides as building blocks

The α-helix can be viewed as a covalent polymeric chain of short peptides. An immediate inspiration from this would be to build artificial supramolecular helices using short peptides. However, short peptides (<8 residues) mainly assemble into ordered nanostructures via β-sheet organization.[44–47] Another feature of the α-helix is its basic structural fragment, the α-turn, which defines the helical conformation of intrinsic helicity. This suggests that helical short peptides could be potential building blocks for artificial supramolecular helices. In the case that well-designed head-to-tail intermolecular interactions would bridge the helical short peptides into supramolecular helices, the propagation of helicity of the short peptide backbone could well take place to cooperatively enhance the interactions between the building blocks and thereby facilitate the formation of a supramolecular helix of high stability.

In 2015, Gazit and colleagues[48] designed a minimal heptad peptide module **27** (Fig. 10a) for supramolecular helical assembly
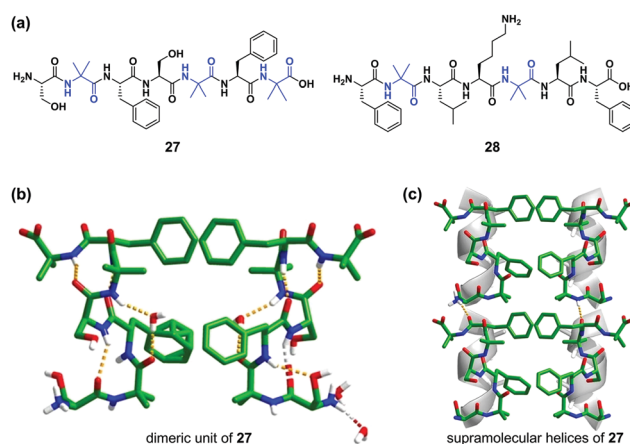

Fig. 10 (a) Molecular structures of peptides **27** and **28** in which the Aib residues that lead to the helical conformation are illustrated in blue. (b) Crystal structure of the hydrogen-bonded helical conformation of **27**, which forms dimeric units through aromatic–aromatic interactions. (c) Crystal structure of zipper-like supramolecular helices from dimeric units of **27** through intermolecular hydrogen bonding. Adapted with permission from ref. 48. Copyright 2015 Springer Nature.

in which non-coded α-aminoisobutyric acid (Aib) residues induced the helical conformation of the short peptide, while phenylalanine residues enhanced dimerization through aromatic–aromatic interactions, followed by intermolecular hydrogen bonding that leads to helical fibrillar assemblies in a phosphate buffer of pH 7.4. The crystal structure of **27** shows that it adopts a helical conformation with two intramolecular i and $i + 3$ hydrogen bonds. One water molecule interacts with the peptide backbone through hydrogen bonding between the NH and CO groups at the i and $i + 3$ positions, respectively, resulting in a continuous hydrogen-bonding network that stabilizes the helical conformation of the heptad peptide (Fig. 10b), reminiscent of the 3_{10} helical structure. Two molecules of **27** form a dimeric unit through aromatic–aromatic interactions between the phenylalanine side chains in a parallel orientation (Fig. 10b). Head-to-tail hydrogen bonds between the terminal amine and internal amide groups bring the dimeric units into supramolecular helices of zipper-like structures (Fig. 10c). This result defines a new design strategy for developing supramolecular helices using helical short-peptides as building blocks. Moreover, subtle modification of the heptad sequence by inclusion of one positively charged lysine residue produces a DNA-binding peptide **28** in a helical conformation and shows a superior DNA condensation and protection efficiency, attributed to the cooperative effects of the helicity, the hydrophobicity, π–π stacking, and electrostatic interactions.

Insertion of β- and γ-amino acid residues into an oligopeptide backbone could lead to predictable helical structures.[49,50] Gopi *et al.*[51] designed α,γ-hybrid tripeptides **29** and **30** (Fig. 11a) that consist of terminal 4- and 3-pyridinyl groups, respectively, aiming to build functional metal–helix frameworks. Both the tripeptides adopt right-handed 12-helix structures that are stabilized by two intramolecular consecutive 12-membered ring hydrogen bonds (Fig. 11a) because of the α,γ-hybrid backbone and helix-favouring Aib residues. In crystals of the **29**/AgBF₄ complex, the 12-helix structure of **29** remains (Fig. 11b). Along the vertical direction, head-to-tail intermolecular hydrogen bonding links helical **29** molecules into a supramolecular helical polymer. Together with the head-to-tail coordination of Ag⁺ to both C- and N-terminal pyridines, which drives the helical polymerization along the horizontal direction, a porous metal–helix framework is formed (Fig. 11c), with a pore size of 5.9 Å that is capable of capturing the greenhouse gas CO_2. However, **30**, which bears 3-pyridinyl metal-binding ligands, adopts a left-handed helical conformation with only one intramolecular 12-membered ring hydrogen bond and forms a 2:2 macrocyclic structure with Ag⁺ (Fig. 11d). This difference demonstrates the role that the coordination sites play in driving the formation of metal-coordinated frameworks, which may relate to the efficient propagation of helicity of the helical peptides when good coordination with metal ions is allowed to drive the formation of supramolecular helices.

Recently, Gopi and co-workers[52] reported that even in the absence of the sterically constrained Aib residues and in the presence of two β-sheet-promoting Val residues, the α,γ-hybrid tripeptide **31** adopts a right-handed 12-helix structure, similar to **29** and **30**. Helical peptide **31** forms metallogels with Ag⁺ and Cu²⁺. Crystals of the **31**/AgBF₄ complex obtained in the gel
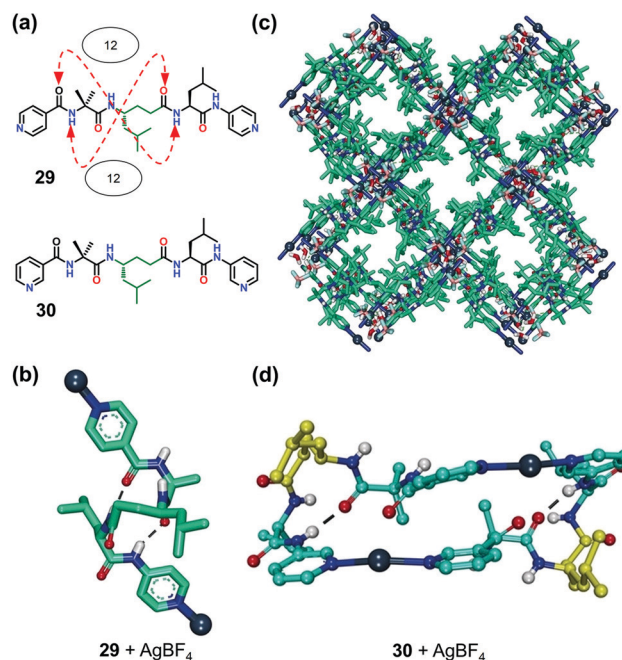

Fig. 11 (a) Molecular structures of α,γ-hybrid peptides **29** and **30** and hydrogen-bonding pattern in **29** of the 12-helix. (b) Crystal structure of **29** with AgBF₄. (c) Porous framework of **29** with AgBF₄ through intermolecular head-to-tail hydrogen bonding and metal coordination interactions in the crystal packing. (d) Crystal structure of a 2:2 macrocycle from **30** binding to AgBF₄. Adapted with permission from ref. 51. Copyright 2019 Wiley-VCH.
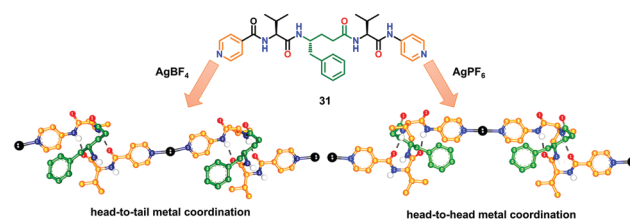

Fig. 12 Head-to-tail metal coordination of α,γ-hybrid peptide **31** with AgBF₄, while head-to-head metal coordination with AgPF₆ is observed in the crystal packing. Adapted with permission from ref. 52. Copyright 2021 Wiley-VCH.

matrix show a head-to-tail Ag⁺ coordination that connects helical **31** into a supramolecular helical chain (Fig. 12), leading to a 2D metal-coordinated network of helices. However, when AgPF₆ is used as the source of metal cations, head-to-head and tail-to-tail coordination of Ag⁺ with **31** mediate the crystal packing (Fig. 12), so that a 3D porous polymer is formed in which no supramolecular helix is identified. It thus appears that in the case of using metal coordination as a driving force, the counter anion plays a role, although its function remains to be clarified.

The azapeptide is another well-known structural motif for helical peptides. We recently developed a series of helical azapeptides from a short peptide-based *N*-amidothiourea motif in which a folded β-turn structure exists in both the solid state and the solution phase (Fig. 13a).[53,54] The helical azapeptides
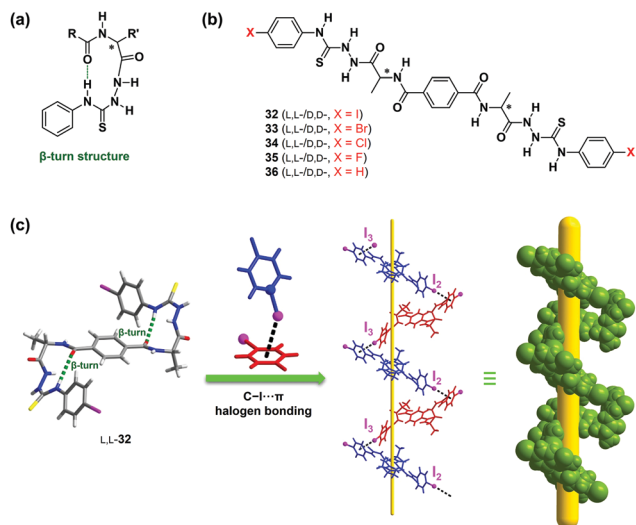
Fig. 13 (a) β-Turn structure in azapeptides from short peptide-based *N*-amidothiourea molecules. (b) Molecular structure of bilateral alanine-based *N*-amidothiourea molecules **32–36**. The asterisks indicate chiral carbons. (c) Crystal structure of single-stranded supramolecular *M*-helix from ʟ,ʟ-**32** through C–I···π halogen bonding. Dashed green lines highlight intramolecular hydrogen bonds for β-turn structures. Dashed black lines highlight C–I···π halogen bonds. Adapted with permission from ref. 55. Copyright 2017 American Chemical Society.

now show potential as helical building blocks for supramolecular helices, when suitable intermolecular interactions are allowed. In 2017 we designed[55] alanine-based bilateral I-substituted *N*-amidothiourea molecules (ʟ,ʟ- and ᴅ,ᴅ-**32**, Fig. 13b) as helical azapeptides in which two helical β-turn structures exist in a *trans*-form with respect to the central benzene ring (Fig. 13c). A single-stranded supramolecular *M*-helix of ʟ,ʟ-**32** forms in both the solid state and dilute CH$_3$CN solution, with a helical pitch of 17.6 Å in which the helical molecules **32** interact *via* inter-molecular head-to-tail C–I···π halogen bonding (Fig. 13c) so that the iodophenyl group at one end of the molecule is a halogen-bonding donor (iodine atom), while that at the other end is the acceptor (phenyl π-system). The calculated inter-action energies of the intermolecular C–I···π halogen bonding, 22.4 kJ mol^{-1} (C–I$_2$···π) and 28.6 kJ mol^{-1} (C–I$_3$···π), are stronger than the C–I···π interaction between two iodobenzene molecules (15.2 kJ mol^{-1}), indicating that the halogen bonding is enhanced by the efficient propagation of the helicity of the β-turn structures. This also results in a high anisotropic *g*-factor (-3×10^{-3}). Moreover, the enantiomeric mixtures of ʟ,ʟ- and ᴅ,ᴅ-**32** in CH$_3$CN exhibit a positive non-linear CD-ee dependence, indicative of the "majority-rules effect", showing that chiral ampli-fication occurs. This means a homochiral preference during the formation of the single-stranded supramolecular helices from the mixtures of ʟ,ʟ- and ᴅ,ᴅ-**32**, governed by propagation of the helicity of the helical β-turn structures. By contrast, the counterparts **33–35**, which contain Br, Cl, or F of lower halogen-bonding ability, or compound **36** with no halogen atom exist in their monomer forms in CH$_3$CN.

The Br-substituted compound **33** of lower intermolecular halogen bonding was found, when dissolved in poor solvent H$_2$O,

to form supramolecular helical fibers, whereas the I-derivative **32** formed non-helical aggregates that precipitate from the solution, but derivatives **34–36** remained in their monomer forms.[56] The moderate halogen-bonding ability and hydrophobicity are assumed to be the reasons for the aggregation behavior of **33**. It is interesting to point out that the supramolecular chirality of the aggregates of **33** in H$_2$O shows an uncommon negative non-linear CD-ee dependence, opposite to that observed for the I-substituted **32** in CH$_3$CN. Hierarchical assembly through head-to-tail C–Br···π halogen bonding within the same helix and hydrophobic interactions between the helices are proposed to rationalize the observed CD-ee dependence of the aggregates of **33** in H$_2$O. These results confirm that halogen bonding can be used well to build supramolecular helices from helical building blocks, with unexpected outcomes when in combination with other inter-molecular interactions.

Later, we[57] succeeded in building a supramolecular double helix, using homochiral bilateral *N*-(*p*-iodobenzoyl)alanine-based amidothiourea molecules (ʟ,ʟ- and ᴅ,ᴅ-**37**, Fig. 14) as helical building blocks in which the two helical β-turns are shown to enhance the intermolecular interactions so that their helicity is well propagated, while the two terminal iodine atoms allow intermolecular crossed double halogen-bonding to support the helix. Although thermodynamically unfavoured, ʟ,ʟ-**37** in its folded *cis*-conformation assembles into the supramolecular *P*-double helix with a pitch of 26.0 Å, *via* intermolecular double and crossed C–I···S halogen bonds, in both the solid state and highly dilute CH$_3$CN solution (Fig. 14). The interaction patterns in this artificial double helix of ʟ,ʟ-**37** are such that the helix is formed by non-covalent halogen bonding, while the two strands are intertwined by the covalent *p*-phenylenediamine linkage, different from those in the natural DNA double helix in which the two covalent strands are cross-linked by multiple base-paring non-covalent hydrogen bonds. The formed supramolecular double helix of ʟ,ʟ-**37** exhibits a high supramolecular helicity with a *g*-factor of -1.6×10^{-2} and a
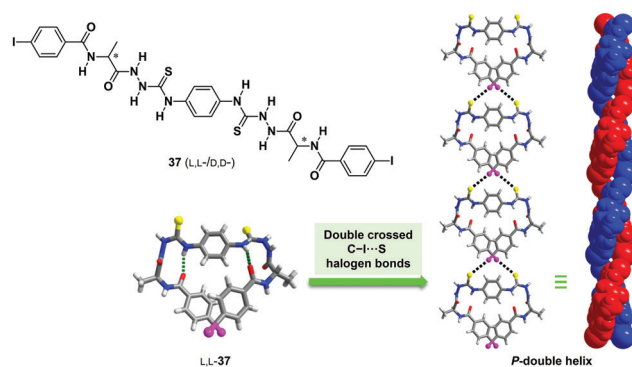

Fig. 14 Molecular structure of bilateral *N*-(*p*-iodobenzoyl)alanine based amidothiourea molecules (ʟ,ʟ- and ᴅ,ᴅ-**37**) and crystal structure of the supramolecular *P*-double helix formed by the *cis*-form ʟ,ʟ-**37** through double crossed C–I···S halogen bonds. The asterisks in the structures indicate the chiral carbons. Dashed green lines highlight intramolecular hydrogen bonds for β-turn structures. Dashed black lines highlight C–I···S halogen bonds. Adapted with permission from ref. 57. Copyright 2019 Springer Nature.

high stability so that it exists in CH$_3$CN at an extremely low concentration of 0.08 μM and remains stable, as indicated by the CD signals, at a high temperature of at least 75 °C. A positive cooperativity of the double crossed halogen-bonding and the good propagation of the helicity of the helical building block was concluded to be responsible for these observations. This also leads to a spontaneous resolution in the formed double helix, so that the CD-ee dependence is linear in CH$_3$CN.

Note that in the formed supramolecular double helix of **37**, the helical azapeptide takes the thermodynamically unfavoured *cis*-form to allow the intermolecular crossed double C–I···S halogen bonding, whereas azapeptide **32** takes its thermo-dynamically favoured *trans*-form in the formed single-strand helix. This means that **37** experiences a change in its conformation during the formation of the double helix, and the penalty to take the unfavoured conformation in its monomer form is paid back by the supramolecular assembly. This conformational change may also contribute to the higher supramolecular helicity and thermo-stability, and the more favoured homochirality of the double helix of **37** compared with the single-strand helix from **32**.

We recently showed that chalcogen bonding is able to drive the formation of supramolecular helices from helical building blocks.[58] The azapeptide that contains a β-turn structure is equipped with a thiophene group, a chalcogen bond donor,[59] at the N- (**38**) and C-terminus (**39**), respectively. While **38** forms a supramolecular *M*-helix of 8.16 Å in pitch *via* intermolecular S···S chalcogen bonding between the thiophene and thiourea moieties, **39** forms a *P*-helix with a pitch of 8.71 Å through S···O chalcogen bonding between the thiophene and amino acid amide groups (Fig. 15). Differences in the supramolecular helices of **38** and **39**, in terms of the chalcogen bonding pattern and helix handedness, are attributed to a more efficient propagation of the helicity of the β-turn structure, when more atoms around the β-turn structure are included in the helical chain.

It appears that a short peptide in helical conformation is able to undergo helical polymerization through intermolecular interactions in a head-to-tail fashion. Yet, reaching stable helical structures from short peptides remains challenging. Fujita and co-workers[60] recently developed an alternative way, the folding-and-assembly strategy (Fig. 16a), to build peptidic nanostructures using flexible short peptides. These peptides fold into a helical conformation upon metal coordination and thereafter assemble into well-defined entangled nanostructures, such as knots,[61] catenanes,[62] β-barrels[63] and coordination networks.[64,65] In 2014
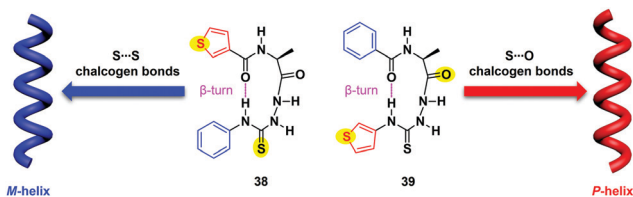
Fig. 15 Supramolecular *M*-helix formed from **38** through S···S chalcogen bonds, while the *P*-helix is formed from **39** through S···O chalcogen bonds. Adapted with permission from ref. 58. Copyright 2021 Royal Society of Chemistry.
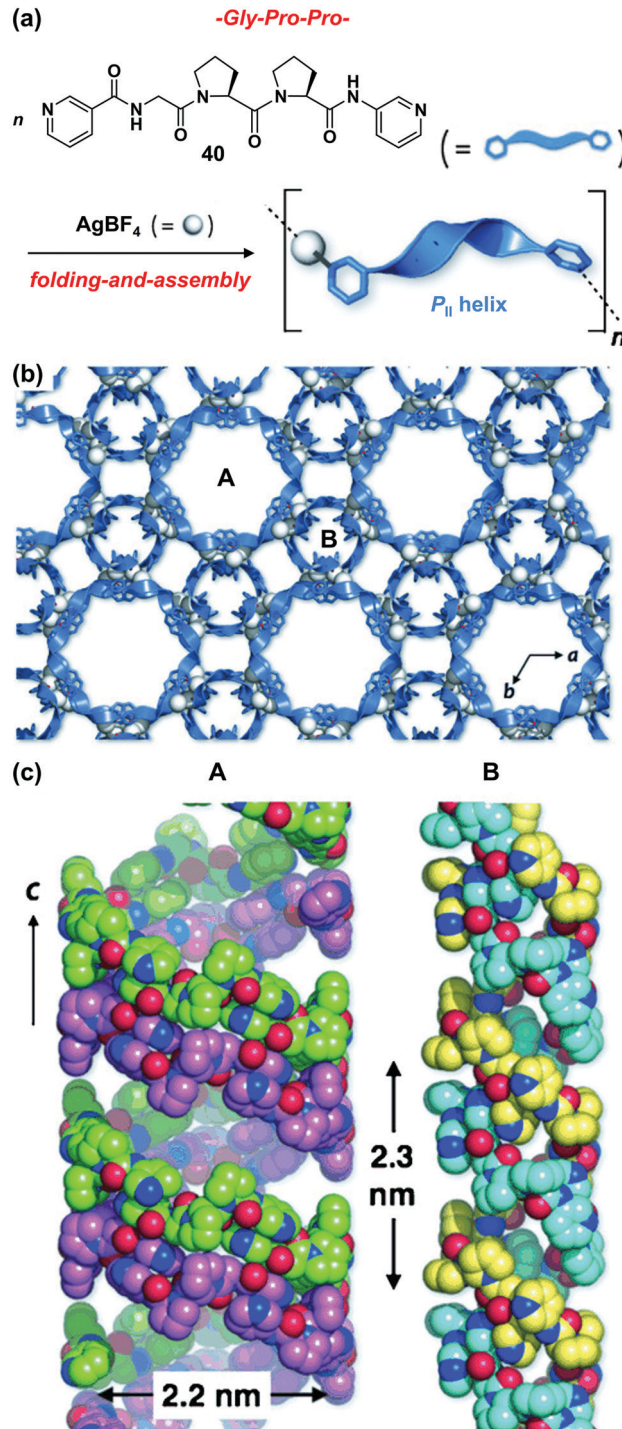
Fig. 16 (a) Coordination of Gly–Pro–Pro ligand **40** with AgBF$_4$ in a folding-and-assembly manner. (b) Hexagonally entangled porous network of [(AgBF$_4$)·**40**]$_n$ in the crystalline state. (c) Space-filling representation of the crystal structures of helical channels A and B. Adapted with permission from ref. 64. Copyright 2014 Wiley-VCH.

they designed[64] a short peptide **40** of Gly–Pro–Pro sequence that is equipped with 3-pyridinyl groups at both the N- and C-termini, which exists in random flexible conformations in solution. Once crystallized with AgBF$_4$, short peptide **40** is fixed into a stable

polyproline II helix (P_{II} helix) conformation (Fig. 16a), and assembles into a hexagonally entangled porous network (Fig. 16b). In that network, helical **40** forms left-handed single helical strands, through pyridinyl–Ag$^+$–pyridinyl coordination in a head-to-tail pattern along the *a*- and *b*-axes, as well as helical channels (large channel A and small channel B) of left-handed duplex-like structures of a helical pitch of 22.8 Å, which are stabilized by π–π stacking of the pyridinyl groups along the *c*-axis (Fig. 16c). Channel A effectively recognizes organic chiral molecules and bio-oligomers, whereas channel B recognizes anions. For example, large channel A is good at chiral recognition of 1,1′-bi-2-naphthol, occurring on the interior surface of the helical channel. Replacement of the counter anion or modification of the amino acid residue leads to a different channel size, whereas the P_{II} helix conformation of the short peptide sequence and the supramolecular helical structures remain.[65] We assume that propagation of the helicity of the P_{II} helix might play a vital role in the folding-and-assembly processes, which in turn promotes the formation of supramolecular helical strands and channels, and therefore the porous network. This might share a similar mechanism with the folding and helical assembly of *m*PE oligomers upon imine metathesis or coordinating to Pd^{2+}.[23–27]

Longer helical short peptides could also function as building blocks for supramolecular helices. In 2016 Schmuck *et al.*[66] designed a β-sheet-featured alanine octamer **41** that consists of alternating D- and L-amino acids with an N-terminal guanidiniocarbonylpyrrole (GCP) group. Octamer **41** self-assembles into a supramolecular β-helix in pure water at pH 5.0, *via* hydrogen bonding-assisted electrostatic interactions between the GCP cation of one peptide and the carboxylate anion of another one in a head-to-tail pattern in which the helicity of the β-sheet is propagated (Fig. 17). Governed by a nucleation–elongation mechanism, the β-helices further aggregate into fibrous structures upon aging for 8 days. Changing the solution pH from 5 to 10, the fibers are transformed into vesicles, ascribed to the deprotonation

of GCP–guanidine at the basic pH. This conversion is pH-switchable, allowing the fabrication of pH-responsive materials.

Compared with helical aromatic building blocks, helical short peptides are more easily accessible in terms of synthesis and share more similarity with the α-helix because of their amino acid constituent motifs. Homochiral elongation is favoured in the formation of the supramolecular helices from helical short peptides because of the ready propagation of the helicity. This could be of help to the understanding of the homochirality in the α-helix, and even the origin of natural homochirality. However, the absence of a large pore structure in the building block backbone makes helical short peptides unable to form hollow helices with channel activity through simple head-to-tail linkages, unless a sophisticated assembly process allows a 3D matrix to be formed, *e.g.*, a 3D coordination network with metal ions, which is established to maintain the helical channels from helical short peptides,[51,52,64,65] for which the transport activities deserve to be explored.

Concluding remarks

Although extensive studies have been carried out on building supramolecular helices, the formation, understanding and applications of supramolecular helices from helical building blocks remain at an early stage. We summarized here some of the examples of supramolecular helices built from helical aromatic foldamers and helical short peptides, to draw a framework picture of the structures of helical building blocks and the resultant supramolecular helices. One issue that remains systematically unexplored is the size of the helical building block: how many blocks does a full turn constitute? Despite being hard to relate the structure of the building block and the structure of the resultant supramolecular helix, the propagation of helicity of the helical building block is proposed to promote the formation of supramolecular helices, probably with homochirality when a pair of enantiomers is employed. The examples that demonstrate folding-driven helical assembly,[24,27,29,64,65] enhanced intermolecular interactions between helical building blocks,[55,57] and chiral amplification[28,29,31,37,38,55,57] illustrate well the operation of the propagation of helicity.

For the work to be done, while the synthesis of helical building blocks, such as aromatic foldamers and peptides is at a more mature stage, molecular design could be a key point for the development of supramolecular helices in a rational way. To facilitate the formation of supramolecular helices, while the helicity is well propagated, the helical backbone should be long enough to allow sufficient intrinsic helicity. In this context, the backbone that can itself fold into a full helical turn could be a better structural motif for developing helical building blocks. While the cavity structure prevails in helical aromatic foldamers that can provide diverse functions in terms of molecular encapsulation, recognition and transportation, it is absent in the helical short peptide backbone. The introduction of cavity-favouring aromatic foldamer backbones into helical short peptides could be a design to be explored, so that hybrids bearing cavity structural
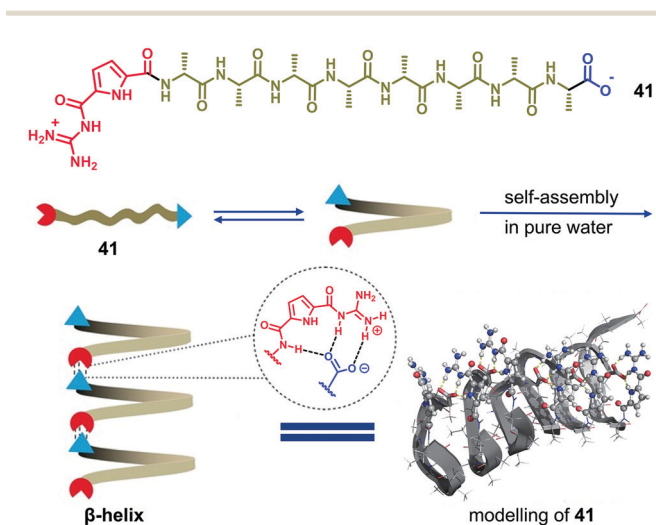

Fig. 17 Supramolecular β-helix formed from peptide **41** of β-sheet structure through ion-pairing hydrogen bonding between the N-terminal guanidiniocarbonylpyrrole cation of one peptide and the C-terminal carboxylate anion of another. Adapted with permission from ref. 66. Copyright 2016 Wiley-VCH.

motifs can afford diverse supramolecular helical structures and functions. Furthermore, the introduction of suitable binding sites that afford matched intramolecular interactions could be another breakthrough for developing stable supramolecular helices from helical building blocks. To allow better propagation of the helicity of the helical backbone, directional interactions could be employed to facilitate the formation of the supramolecular helices. In addition to often-employed π–π stacking, hydrogen bonding and metal coordination, attractive σ-hole-based interactions such as halogen and chalcogen bonds are promising candidates to act as alternative driving forces to support the supramolecular helices. Using building block molecules that can be made into helices upon intermolecular interactions, which lead to supramolecular helices, is a route that deserves more attention. This can also be done by introducing structural elements into the building block molecule so that it is encouraged to adopt a helical conformation using a subtle external stimulus. The majority of supramolecular helices presented here are fabricated in organic solvents. It is thus expected that using a sophisticated combination of the intermolecular interactions, these helices could be made stable in aqueous solutions so that feasible applications can be explored.

One the other hand, comprehensive characterization strategies are in high demand. X-Ray crystallography is the most powerful tool to provide unambiguous evidence of the supramolecular structure. However, it is still difficult to obtain crystals from all of these supramolecular systems, while structures in the solution phase may be different from those in the crystalline state.[67] Therefore, methods such as CD, NMR, and electron microscopy as well as theoretical calculations should also be established to investigate the conformation of building blocks, intermolecular interactions and supramolecular helical structures, so that possible cooperative effects between the intra- and inter-molecular interactions can be identified.

Moreover, the functions of the formed supramolecular helices are intriguing. Encouragingly, such supramolecular helices can afford helical channels that have shown successful applications in molecular encapsulation, recognition and transportation. While the artificial lipid membrane has been extensively studied to measure the trans-membrane activity, the capacity of transporting species across real biomembranes should be the focus of future efforts. Due to the chiral nature of these channels, applications in chiral recognition, catalysis and chiral structural analysis[68] are promising subjects. The propagation of helicity is able to drive the homochiral elongation of the supramolecular helix, such that it is possible to enable spontaneous resolution for conglomerate formation, an important new way of purifying chiral compounds. Furthermore, the cooperativity between the propagation of helicity and the intermolecular interactions would lead to high supramolecular helicity of supramolecular helices from helical building blocks, which is helpful in creating chiral functional materials with a high luminescence dissymmetry factor.[69]

We hope this feature article can draw more attention from the supramolecular community towards supramolecular helices, built using helical and/or made-helical building blocks, thereby allowing the rational design, better understanding and broad applications of structurally diverse functional supramolecular helices.

Conflicts of interest

There are no conflicts to declare.

Acknowledgements

Notes and references

1 E. Yashima, N. Ousaka, D. Taura, K. Shimomura, T. Ikai and K. Maeda, *Chem. Rev.*, 2016, **116**, 13752–13990.
2 J. D. Watson and F. H. C. Crick, *Nature*, 1953, **171**, 737–738.
3 L. Pauling, R. B. Corey and H. R. Branson, *Proc. Natl. Acad. Sci. U. S. A.*, 1951, **37**, 205–211.
4 S. Cantekin, T. F. A. de Greef and A. R. A. Palmans, *Chem. Soc. Rev.*, 2012, **41**, 6125–6137.
5 F. Helmich, M. M. Smulders, C. C. Lee, A. P. Schenning and E. W. Meijer, *J. Am. Chem. Soc.*, 2011, **133**, 12238–12246.
6 F. Würthner, C. R. Saha-Möller, B. Fimmel, S. Ogi, P. Leowanawat and D. Schmidt, *Chem. Rev.*, 2016, **116**, 962–1052.
7 A. Lohr and F. Würthner, *Angew. Chem., Int. Ed.*, 2008, **47**, 1232–1236.
8 L. Pérez-García and D. B. Amabilino, *Chem. Soc. Rev.*, 2002, **31**, 342–356.
9 A. R. A. Palmans and E. W. Meijer, *Angew. Chem., Int. Ed.*, 2007, **46**, 8948–8968.
10 X. Yan, Q. Wang, X. Chen and Y.-B. Jiang, *Adv. Mater.*, 2020, **32**, 1905667.
11 Q.-H. Guo, Y. Jiao, Y. Feng and J. F. Stoddart, *CCS Chem.*, 2021, **3**, 1542–1572.
12 A. G. Shtukenberg, Y. O. Punin, A. Gujral and B. Kahr, *Angew. Chem., Int. Ed.*, 2014, **53**, 672–699.
13 M. J. Bierman, Y. K. A. Lau, A. V. Kvit, A. L. Schmitt and S. Jin, *Science*, 2008, **320**, 1060–1063.
14 A. Ben-Moshe, A. da Silva, A. Müller, A. Abu-Odeh, P. Harrison, J. Waelder, F. Niroui, C. Ophus, A. M. Minor, M. Asta, W. Theis, P. Ercius and A. P. Alivisatos, *Science*, 2021, **372**, 729–733.
15 I. Popov, *Science*, 2021, **372**, 688.
16 A. S. Mahadevi and G. N. Sastry, *Chem. Rev.*, 2016, **116**, 2775–2825.
17 S. H. Gellman, *Acc. Chem. Res.*, 1998, **31**, 173–180.
18 D. J. Hill, M. J. Mio, R. B. Prince, T. S. Hughes and J. S. Moore, *Chem. Rev.*, 2001, **101**, 3893–4012.
19 D.-W. Zhang, X. Zhao, J.-L. Hou and Z.-T. Li, *Chem. Rev.*, 2012, **112**, 5271–5316.
20 D.-W. Zhang, X. Zhao and Z.-T. Li, *Acc. Chem. Res.*, 2014, **47**, 1961–1970.
21 Y. Ferrand and I. Huc, *Acc. Chem. Res.*, 2018, **51**, 970–977.
22 J. C. Nelson, J. G. Saven, J. S. Moore and P. G. Wolynes, *Science*, 1997, **277**, 1793–1796.
23 K. Oh, K.-S. Jeong and J. S. Moore, *Nature*, 2001, **414**, 889–893.
24 D. Zhao and J. S. Moore, *J. Am. Chem. Soc.*, 2002, **124**, 9996–9997.
25 D. Zhao and J. S. Moore, *J. Am. Chem. Soc.*, 2003, **125**, 16294–16299.
26 M. T. Stone and J. S. Moore, *J. Am. Chem. Soc.*, 2005, **127**, 5928–5935.
27 J. W. Wackerly and J. S. Moore, *Macromolecules*, 2006, **39**, 7269–7276.
28 L. Brunsveld, E. W. Meijer, R. B. Prince and J. S. Moore, *J. Am. Chem. Soc.*, 2001, **123**, 7978–7984.
29 Y. Wang, F. Li, Y. Han, F. Wang and H. Jiang, *Chem. – Eur. J.*, 2009, **15**, 9424–9433.
30 L. A. Cuccia, J.-M. Lehn, J.-C. Homo and M. Schmutz, *Angew. Chem., Int. Ed.*, 2000, **39**, 233–237.
31 S. Azeroual, J. Surprenant, T. D. Lazzara, M. Kocun, Y. Tao, L. A. Cuccia and J.-M. Lehn, *Chem. Commun.*, 2012, **48**, 2292–2294.

32 T. Yan, F. Yang, S. Qi, X. Fan, S. Liu, N. Ma, Q. Luo, Z. Dong and J. Liu, *Chem. Commun.*, 2019, **55**, 2509–2512.
33 C. Lang, X. Deng, F. Yang, B. Yang, W. Wang, S. Qi, X. Zhang, C. Zhang, Z. Dong and J. Liu, *Angew. Chem., Int. Ed.*, 2017, **56**, 12668–12671.
34 S. Qi, C. Zhang, H. Yu, J. Zhang, T. Yan, Z. Lin, B. Yang and Z. Dong, *J. Am. Chem. Soc.*, 2021, **143**, 3284–3288.
35 D. Bai, T. Yan, S. Wang, Y. Wang, J. Fu, X. Fang, J. Zhu and J. Liu, *Angew. Chem., Int. Ed.*, 2020, **59**, 13602–13607.
36 C. Zhang, X. Deng, C. Wang, C. Bao, B. Yang, H. Zhang, S. Qi and Z. Dong, *Chem. Sci.*, 2019, **10**, 8648–8653.
37 H. Zhao, W. Q. Ong, F. Zhou, X. Fang, X. Chen, S. F. Y. Li, H. Su, N.-J. Cho and H. Zeng, *Chem. Sci.*, 2012, **3**, 2042–2046.
38 H. Zhao, S. Sheng, Y. Hong and H. Zeng, *J. Am. Chem. Soc.*, 2014, **136**, 14270–14276.
39 Y. Huo and H. Zeng, *Acc. Chem. Res.*, 2016, **49**, 922–930.
40 L. C. Gilday, S. W. Robinson, T. A. Barendt, M. J. Langton, B. R. Mullaney and P. D. Beer, *Chem. Rev.*, 2015, **115**, 7118–7195.
41 G. Cavallo, P. Metrangolo, R. Milani, T. Pilati, A. Priimagi, G. Resnati and G. Terraneo, *Chem. Rev.*, 2016, **116**, 2478–2601.
42 C.-Z. Liu, S. Koppireddi, H. Wang, D.-W. Zhang and Z.-T. Li, *Angew. Chem., Int. Ed.*, 2019, **58**, 226–230.
43 S. Koppireddi, C.-Z. Liu, H. Wang, D.-W. Zhang and Z.-T. Li, *CrystEngComm*, 2019, **21**, 2626–2630.
44 X. Yan, J. Blacklock, J. Li and H. Möhwald, *ACS Nano*, 2012, **6**, 111–117.
45 W. J. M. FrederixPim, G. G. Scott, Y. M. Abul-Haija, D. Kalafatovic, C. G. Pappas, N. Javid, N. T. Hunt, R. V. Ulijn and T. Tuttle, *Nat. Chem.*, 2015, **7**, 30–37.
46 S. Kim, J. H. Kim, J. S. Lee and C. B. Park, *Small*, 2015, **11**, 3623–3640.
47 Z. Luo and S. Zhang, *Chem. Soc. Rev.*, 2012, **41**, 4736–4754.
48 S. Mondal, L. Adler-Abramovich, A. Lampel, Y. Bram, S. Lipstman and E. Gazit, *Nat. Commun.*, 2015, **6**, 8615.
49 S. H. Choi, I. A. Guzei, L. C. Spencer and S. H. Gellman, *J. Am. Chem. Soc.*, 2008, **130**, 6544–6550.
50 B. F. Fisher and S. H. Gellman, *J. Am. Chem. Soc.*, 2016, **138**, 10766–10769.

51 R. Misra, A. Saseendran, S. Dey and H. N. Gopi, *Angew. Chem., Int. Ed.*, 2019, **58**, 2251–2255.
52 S. Dey, R. Misra, A. Saseendran, S. Pahan and H. N. Gopi, *Angew. Chem., Int. Ed.*, 2021, **60**, 9863–9868.
53 X.-S. Yan, K. Wu, Y. Yuan, Y. Zhan, J.-H. Wang, Z. Li and Y.-B. Jiang, *Chem. Commun.*, 2013, **49**, 8943–8945.
54 X.-S. Yan, H. Luo, K.-S. Zou, J.-L. Cao, Z. Li and Y.-B. Jiang, *ACS Omega*, 2018, **3**, 4786–4790.
55 J. Cao, X. Yan, W. He, X. Li, Z. Li, Y. Mo, M. Liu and Y.-B. Jiang, *J. Am. Chem. Soc.*, 2017, **139**, 6605–6610.
56 X. Yan, J. Cao, Y. Zhang, P. Weng, D. Miao, Z. Zhao, Z. Li and Y.-B. Jiang, *Chem. Commun.*, 2021, **57**, 1802–1805.
57 X. Yan, K. Zou, J. Cao, X. Li, Z. Zhao, Z. Li, A. Wu, W. Liang, Y. Mo and Y. Jiang, *Nat. Commun.*, 2019, **10**, 3610.
58 D. Shi, J. Cao, P. Weng, X. Yan, Z. Li and Y.-B. Jiang, *Org. Biomol. Chem.*, 2021, **19**, 6397–6401.
59 P. Scilabra, G. Terraneo and G. Resnati, *Acc. Chem. Res.*, 2019, **52**, 1313–1324.
60 T. Sawada and M. Fujita, *Chem*, 2020, **6**, 1861–1876.
61 Y. Inomata, T. Sawada and M. Fujita, *Chem*, 2020, **6**, 294–303.
62 T. Sawada, M. Yamagami, K. Ohara, K. Yamaguchi and M. Fujita, *Angew. Chem., Int. Ed.*, 2016, **55**, 4519–4522.
63 M. Yamagami, T. Sawada and M. Fujita, *J. Am. Chem. Soc.*, 2018, **140**, 8644–8647.
64 T. Sawada, A. Matsumoto and M. Fujita, *Angew. Chem., Int. Ed.*, 2014, **53**, 7228–7232.
65 T. Sawada, M. Yamagami, S. Akinaga, T. Miyaji and M. Fujita, *Chem. – Asian J.*, 2017, **12**, 1715–1718.
66 M. Li, M. Radić Stojković, M. Ehlers, E. Zellermann, I. Piantanida and C. Schmuck, *Angew. Chem., Int. Ed.*, 2016, **55**, 13015–13018.
67 B. Yang, J.-W. Zhang, S.-B. Yu, Z.-K. Wang, P.-Q. Zhang, X.-D. Yang, Q.-Y. Qi, G.-Y. Yang, D. Ma and Z.-T. Li, *Sci. China: Chem.*, 2021, **64**, 1228–1234.
68 A. Saito, T. Sawada and M. Fujita, *Angew. Chem., Int. Ed.*, 2020, **59**, 20367–20370.
69 T. Zhao, J. Han, P. Duan and M. Liu, *Acc. Chem. Res.*, 2020, **53**, 1279–1292.